Carbohydrate Polymers 88 (2012) 239–249

Contents lists available at SciVerse ScienceDirect

Carbohydrate Polymers

journal homepage: www.elsevier.com/locate/carbpol

A novel carboxymethyl chitosan-based folate/Fe_3O_4/CdTe nanoparticle for targeted drug delivery and cell imaging

Jian-Min Shen[a,b], Wan-Jin Tang[a], Xiao-Li Zhang[a], Tong Chen[a], Hai-Xia Zhang[a,*]

[a] Key Laboratory of Nonferrous Metal Chemistry and Resources Utilization of Gansu Province, Lanzhou University, Lanzhou 730000, China
[b] School of Life Sciences, Lanzhou University, Lanzhou 730000, China

ARTICLE INFO

Article history:
Received 14 October 2011
Received in revised form
26 November 2011
Accepted 30 November 2011
Available online 16 December 2011

Keywords:
Carboxymethyl chitosan (CMCH)
Folate
Magnetic nanoparticles (MNPS)
CdTe quantum dots (CdTe QDs)
Drug delivery
Cell imaging

ABSTRACT

We developed a novel folate conjugated carboxymethyl chitosan-ferroferric oxide doped cadmium telluride quantum dot nanoparticles (abbreviate: CFLMNPs). Processing parameters affected the end product properties were optimized systematically. The morphology, composition, and properties of the as-prepared CFLMNPs have also been characterized and determined using TEM, SEM, DLS, FT-IR spectra, EDX, fluorescence spectroscopy, VSM, XRD and LSCM studies. The resulting CFLMNPs possessed intense superparamagnetic effect and photoluminescence (PL) property at room temperature. The size range of CFLMNPs was from 170 to 190 nm under simulate physiological environment. The anticancer drug selected in this study was adriamycin which can be used for the human liver cancer treatment. Under present experiment condition, the loading efficiency of ADM was approximately 36.6 wt% for CFLMNPs. The cumulative release under sink condition mainly occurred for the first 24 h, and could reach 36% at pH 5.3 and 15% at pH 7.4 within 24 h. 85% and 70% of viability of L02 and HepG2 cells were watched at a blank CFLMNPs concentration of 1 mg/mL, respectively. It is found that the CFLMNPs were transported into the HepG2 cells by an folate-receptor-mediated endocytosis mechanism. These results indicate that the multifunctional CFLMNPs possess a high drug loading efficiency, low cytotoxicity and favorable cell compatibility, and are promising candidates for carboxymethyl chitosan-based targeted drug delivery and cellular imaging.

1. Introduction

In recent years, a variety of multifunctional magnetic nanoparticles (MNPs) have been broadly applied in biomedical fields, including drug delivery (Guo, Yang, Wang, He, & Chen, 2006) and cell imaging (Mathew et al., 2010; Myers, Campana, & Shubayev, 2006). It has been feasible to design and prepare multifunctional MNPs with tailored magnetic/luminescent properties based on a specific application purpose (Mangeney et al., 2006). These functional MNPs were synthesized principally through modifying some functional groups on the surface structure of magnetic particles or combining with other functional materials (noble metals, semiconductor, etc.). After further conjugated with specific targeting ligand on the particles, followed by immobilization with anticancer drugs, composites fabricate unique particulate systems that can be taken in by cancer cells to achieve diagnosis and therapeutics.

In order to avoid a propensity to agglomerate, improve stability in medium and facilitate to connect with other functional groups, a proper coating is necessary on the surface of magnetic cores (Saleh et al., 2005). Several available matrixes have been used for cover to MNPs surface, including polystyrene, polyaniline, dodecylamine, sodium oleate, silica and chitosan. Chitosan has been extensively applied (Jayakumar, Menon, Manzoor, Nair, & Tamura, 2010; Muzzarelli et al., 2012; Rejinold, Chennazhi, Tamura, Nair, & Jayakumar, 2011) because of its versatile properties, such as biological functionality, compatibility, safety, biodegradability (Calero, Munoz, Ramírez, & Guerrero, 2010; Corato et al., 2011). Several representative works have revealed the potential applications of magnetic chitosan synthesized by covalent binding, cross linking, and coprecipitation method in environmental remediation (Wang, Peng, Yang, Liu, & Hu, 2011) and drug delivery (Chen, Yang, Ma, & Wu, 2011). In these applications, chitosan supplied a cationic, multifunctional and hydrophilic polymer coating, and the resulting composites were suitable for magnetic bioseparation and drug adsorption. Unfortunately, these magnetic chitosan composites had either an unstable state or nonuniform particle-size distribution because limited solubility of chitosan led to agglomeration. The uncertain status greatly restricted properties and applications of materials, particularly in application served as drug carrier. Jayakumar's group developed a novel drug carrier for the integration of targeting, controlled drug delivery and the imaging of cancer cells using folic acid conjugated CMCH coordinated to quantum

* Corresponding author. Tel.: +86 931 891 2510; fax: +86 931 891 2582.
E-mail address: zhanghx@lzu.edu.cn (H.-X. Zhang).

0144-8617/$ – see front matter © 2011 Elsevier Ltd. All rights reserved.
doi:10.1016/j.carbpol.2011.11.087

dot (Mathew et al., 2010), in which the CMCH as cross-linking agent overcome its disadvantages like limited solubility and lack of effectiveness as absorption enhancer at neutral pH values (Jayakumar, Prabaharan, et al., 2010). If the magnetic nanoparticles are bound to this kind of drug carrier to promote its targeting property, it will be interesting. This is because the drug-loaded magnetic targeting can improve aggressive potential on pathologic sites under external magnetic field, which could decrease drug dosage and reduce the damage to normal cells.

Recently the development of magnetic nanocomposites incorporated with fluorescent marker has become a favorite topic for drug delivery and cell tracking (Gil & Parak, 2008). The magnetic drug carrier labeled fluorescent dye could be tracked to obtain imaging of migration and anchoring of drug in vivo (Cho et al., 2010). CdTe QDs, a semiconductor QDs, possess a number of attractive optical properties (Guo et al., 2006), including high quantum efficiency, long fluorescence lifetime, narrow and symmetric luminescence bands, et al., which makes it possible to become a practical biological probe. However, though pure QDs possess satisfactory PL intensity (Guo, Yang, & Wang, 2005), it is unavoidable for the QDs fluorescence to be weakened even quenched in the course of preparing luminescent/magnetic nanocomposites (Wang et al., 2009). In this work, we conducted some researches about the retaining the fluorescence of QDs in the magnetic chitosan composites as perfect as possible.

Currently, cancer continues to threaten human health. Though various anticancer drugs came into being, conventional chemotherapeutic methods show poor specificity in reaching tumor tissue and are often restricted by dose-limiting toxicity. The magnetic nanoparticles as drug carriers can provide a favorable platform for drug targeting under the effect of external magnetic field. In addition, folate is an effective target ligand due to its high binding affinity with the folate receptors that are over-expressed on human cancer cell membrane including ovarian, lung, breast, prostate and liver cancers (Manzoor, Johny, Menon, & Nair, 2009; Pan & Feng, 2009; Turek, Leamon, & Low, 1993) while only minimally distributed on normal cell surface. Thus, it will be interesting to develop folate-conjugated luminescent/magnetic nanoparticles using CMCH as cross-linking agent to fabricate specific drug carrier. Adriamycin, an anthracycline antibiotic, has potent antitumor activity (Blum & Carter, 1974; Jeong et al., 2009), and was selected as the anticancer drug model molecule for the human liver cancer in this study.

In present study, we prepared CMCH-based folate@luminescent@magnetic nanoparticles with folate receptors affinity, magnetic responsiveness and luminescent property via layer-by-layer assembly technique in situ surface (Fig. 1). A whole set of physicochemical characteristics of the CFLMNPs was investigated. To evaluate performances of the resulting CFLMNPs, drug release behavior and cytotoxicity in vitro were also researched. Human hepatocytes normal L02 cell and cancer HepG2 cells were used to observation of binding and morphological changes in vitro in order to examine antitumor activity of adriamycin-loaded CFLMNPs.

2. Materials and methods

2.1. Materials

Ferric trichloride hexahydrate, ethanediol, sodium acetate, tellurium powder (purity above 99%), polyethyleneglycol-2000 (PEG), sodium borohydride, cadmium chloride (99%), thioglycolic Acid (TGA, 99%), chitosan (80 mesh, MW, 22.4 kDa, deacetylation degree above 95%), sodium hydroxide, 1-ethyl-3-(3-dimethylaminopropyl) carbodiimide hydrochloride (EDAC), N-hydroxysuccinimide (NHS), isopropanol, monochloroacetic acid solution, adriamycin (ADM) were purchased from Sigma. RPMI-1640 medium was obtained from Gibco (USA). Calf serum was acquired from Sijiqing Biological Engineering Materials Co., Ltd., Hangzhou, China. Dimethyl sulfoxide (DMSO) was analytical grade and obtained from Gansu Yinguang Chemical Industry Co. (China). All other chemicals were of analytical grade. The water used in the study was prepared using a Milli-Q Water Purification System (Milli-Pore, Bedford, MA, USA).

2.2. Synthesis of Fe_3O_4@CMCH

A magnetic core of CFLMNPs was prepared as described (Deng et al., 2005; Xu et al., 2006). Chitosan was modified by carboxymethylation (CMCH) according to previous literature reports (Chen & Park, 2003). The binding of CMCH with magnetite nanoparticles was achieved by our optimized method from previous literature (Chang & Chen, 2005): first, at room temperature, 125 mg of CMCH was added to 2.5 mL of PBS (5 mM, pH 7.5) containing 0.1 M NaCl (buffer A) and dissolved under sonication for 30 min. The solution was centrifuged at 1000 rpm for 5 min to remove any impurities. 250 μL of EDAC solution (25 mg/mL in buffer A) was added slowly to the CMCH solution and sonicate for another 10 min to obtain active CMCH. Then, 2.5 mL of Fe_3O_4 suspension (50 mg/mL in buffer A) was added to active CMCH solution and the reaction mixture was sonicated for 5 min followed by vibrating for 2 h at 25 °C to facilitate a binding balance. Coated-CMCH Fe_3O_4 complexes were formed through the reaction of active CMCH with hydroxyl on Fe_3O_4. The product was separated from the reaction mixture with a centrifuge at 6000 rpm for 5 min, and then was washed with water and ethanol several times, followed by drying overnight in a vacuum oven at 60 °C. Finally, the product was fabricated into Fe_3O_4@CMCH suspension (50 mg/mL in buffer A) for further use. The loading amount of CMCH on magnetic beads was measured by deducting unbound CMCH content from added total amount. With respect to the quantification of CMCH content, the major operation steps can be summarized as: acid hydrolysis of CMCH with 6 mol/L HCl under high pressure and heating (0.12 MPa, 120 °C) for 2 h, and determination of total reducing sugar based on literature (Miller, 1959).

2.3. Synthesis of CMCH-coated Fe_3O_4@CMCH@CdTe particles (CLMNPs)

The TGA-capped CdTe quantum dots were synthesized by the hydrothermal route combined with previous literature (Guo et al., 2006). In order to facilitate a binding between CdTe and Fe_3O_4@CMCH, the prepared CdTe nanocrystal was precipitated in excessive anhydrous ethanol, dissolved again in deionized water, and then adjusted pH to 7.5. If not specifically mentioned in the text, CdTe nanocrystal concentrated 10 times was used as the reaction solution. 1.25 mL of EDAC solution (25 mg/mL in buffer A) was added slowly into 8 mL of above CdTe solution irradiated for 24 h in natural light, and the mixture was sonicated for 10 min to obtain active QDs. Then, the amount of Fe_3O_4 in Fe_3O_4@CMCH was kept constant at 0.5 μmol in all cases, while the amount of QDs was varied on the basis of the QD:Fe_3O_4 ratio (0:1, 1:1, 2:1, 5:1, 10:1, 20:1, 40:1), and the reaction mixtures were sonicated for 5 min, followed by vibrating for 4 h at 5 °C. The washing procedure was necessary to completely remove the excessive CdTe in aqueous solution with buffer A. The PL intensity of the Fe_3O_4@CMCH@CdTe particles prepared under the different QD:Fe_3O_4 ratio was measured comparatively. The ratio of QDs to Fe_3O_4 particles as optimization was determined to give consideration to the PL intensity and appropriate dosages of QDs. In order to stabilize CdTe in aqueous solution, 2.5 mL of EDAC-activated CMCH (50 mg/mL, pH 7.5) was

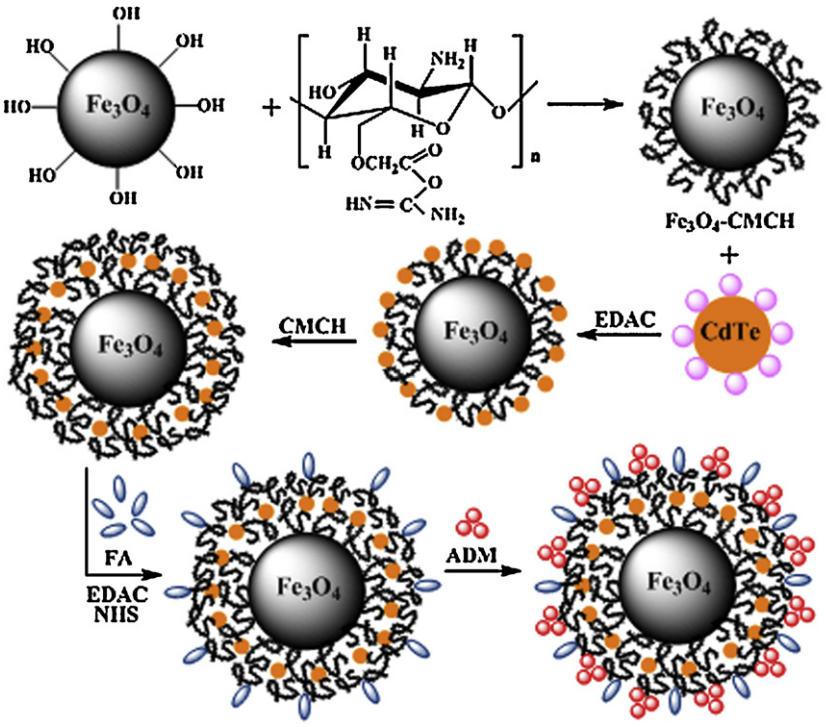

Fig. 1. Schematic diagrams of the fabrication procedure for CMCH-based folate/luminescent/magnetic nanoparticles.

put into 2.5 mL of the performed Fe_3O_4@CMCH@CdTe suspension (50 mg/mL). The mixture was vibrated for 1 h for constructing a CMCH shell on nanoparticles and washed thoroughly with buffer A, followed by freeze drying to obtain dried CLMNPs.

2.4. Formulation of folate-conjugated CLMNPs (CFLMNPs)

Five milliliters of 1 mg/mL solution of folate in PBS buffer (5 mM, pH 6.0, buffer B) was prepared. The carboxyl groups on folate were activated by adding 1.63 mg of EDAC and 1.30 mg of NHS and stirred for 5 h at room temperature. 10 mL of 5 mg/mL CLMNPs was added to the mixture dropwise with stirring and the reaction was carried out in the dark for 8 h. The product, folate-conjugated CLMNPs were washed thoroughly with buffer B, followed by freeze drying to obtain dried CFLMNPs.

2.5. Drug loading and in vitro release

The loading of ADM was achieved as follows: 25 mg of CFLMNPs were added into 30 mL of ADM solution (1 mg/mL in 0.9% NaCl), and shaken for 24 h at room temperature until ADM concentration in the solution stabilized. Then the suspension was centrifuged at 6000 rpm for 10 min. To remove unbound ADM, the nanoparticles were further rinsed three times with 0.9% NaCl, followed by freeze drying. All the supernatants were collected, and the concentration of the unbound ADM was assayed by UV–visible spectrophotometer at 479 nm. The loading efficacy and loading amount of ADM were determined according to the decrease in initial ADM solution. All the experiments were carried out in triplicate.

In order to evaluate the effect of pH on the release mechanism, the release profile of ADM was obtained by sinking 25 mg of ADM-loaded CFLMNPs in 30 mL of PBS (50 mM, pH = 7.4 and pH 5.3) at $37 \pm 1\,^{\circ}C$ in a water bath with gentle shaking. 0.5 mL of sample in the solution was withdrawn by means of magnetic separation at defined time periods and analyzed by UV spectrophotometer at 479 nm. An equal volume of fresh medium was added and the amount of drug released was calculated as described (Fisher, Huddersman, & Taylor, 2003). Each experiment was conducted in triplicate and results are presented as mean (standard deviation).

2.6. In vitro cytotoxicity study

The cytotoxicity of the blank and the ADM-loaded CFLMNPs was assessed by using the MTT assay. L02 cells and HepG2 cells used for these studies were obtained from the cell bank of Shanghai Science Academe (China). The cells (1×10^4 cells/well) were incubated in RPMI-1640 medium containing calf serum (10%) and 1% penicillin–streptomycin in a 96-well plate, in a fully humidified incubator at $37\,^{\circ}C$ with 5% CO_2. When the cells reached 80% confluence with normal morphology, the blank and ADM-loaded CFLMNPs with a concentration of 200, 400, 600, 800 and 1000 μg/mL were added to cell dishes, respectively, and then these cell dishes were put into incubators at $37\,^{\circ}C$ for 12 h. Under these incubation concentrations, no detectable damage to the cells was observed. After incubation for a defined time, the culture medium was removed and 20 μL of MTT reagent (diluted in culture medium, 0.5 mg/mL) was added, followed by incubating for another 2 h. The MTT/medium was removed carefully and DMSO (150 μL) was added to each well for dissolving the formazan crystals. Absorbance of the colored solution was measured at 570 nm using a microplate reader (Bio-Rad, iMark™). All experiments were performed in triplicate.

2.7. Cellular imaging

The laser scanning confocal microscopy (LSCM, Olympus, FV-300, IX71) was used for L02 and HepG2 cell imaging. Two kinds of cells (6×10^4 cells/well) were seeded on a 6-well plate $37\,^{\circ}C$ for 24 h. After that, the blank and ADM-loaded CFLMNPs with a concentration of 200 μg/mL were added to the cell dishes, respectively. After a further 30 min and 60 min incubation, these nanosphere-loaded cells were washed with PBS three times to remove the free nanoparticles attached on the outer surface of cell membrane. The cell targeting was detected on LSCM for luminescence imaging

under excitation wavelength of 405 nm. The cell imaging of three control experiments were also performed: cell alone, HepG2 cells incubated with free ADM, and L02 and HepG2 cells incubated with non-folate conjugated CLMNPs.

2.8. Characterization

UV–vis absorption spectra were measured on an Ultraviolet–visible Spectrophotometer (Puxi TU-1810, Beijing, China). Fluorescence spectra of liquid state and solid state were recorded on a RF-5310 PC spectrofluorophotometer (SHIMADZU) and a FLS920 spectrofluorimeter (Edinburgh, England), respectively. Large-angle powder X-ray diffraction (XRD) patterns from 10° to 80° were recorded at X'Pert PRO (PANalytical, Holand) using Cu Kα radiation. Transmission electron microscopy (TEM) images were measured with a TecnaiG^2 F30 (FEI, USA) by placing one drop of the samples on copper grids coated with carbon. Scanning electron microscopy (SEM) image and X-ray energy dispersive (EDX) spectra were obtained on an S-4800 field emission scanning electron microscope with an EDX spectroscopy (Hitachi, Japan). The Fourier transform infrared (FTIR) spectra were acquired with an FTIR spectrometer (NEXUS 670 FT-IR, Nicolet, USA). The magnetic properties were recorded using a vibrating sample magnetometer (VSM) (Lake Shore, USA). The hydrodynamic diameter of the CFLMNPs was determined by dynamic light scattering (DLS) (BI-200SM, Brookharen Instruments Corporation, USA). The cellular images were acquired with a laser scanning confocal microscope (Olympus, FV-300, IX71). Others also employed in this work were a High-speed refrigerated centrifuge (Himac, CR 21G, Hitachi, Japanese), a sonicator operated at 35 kHz (Elma TI-H-5 MF2, Germany) and level swing bed with temperature controller (Heo Bio-Tech Co., Ltd, Beijing, China).

3. Results and discussion

3.1. Preparation and characterization of Fe_3O_4@CMCH

In this study, we synthesized the uniform magnetic nanoparticles with desired size using the polyalcohol method which has a yield of about 30%. At the same time, the magnetic nanoparticles was fabricated into Fe_3O_4@CMCH. It is found that the coating amount and binding mode of CMCH on magnetic cores were strongly influenced by several elements, predominantly such as initial CMCH concentration, medium pH, reaction time and temperature.

Generally, the coating amount of CMCH increased nonlinearly with increased initial CMCH concentration on equal adsorbent (Fig. 2a). At first, the added CMCH was adsorbed chemically on the Fe_3O_4 surface to form the first CMCH molecule layer through covalent binding between EDAC-activated CMCH with the hydroxyl groups on the Fe_3O_4 surface. Then the excess CMCH was adsorbed physically on the first layer CMCH thus forming a polymer shell. It is worth noting that when the initial CMCH concentration is high enough (50 mg/mL) to form sticky colloid in reaction solution, the resultant Fe_3O_4@CMCH composites aggregated and were unstable due to alternation of covalent binding to physisorption (Chang & Chen, 2005). The clustering fraction sizes were above 500 nm, even larger than 1000 nm. In this work, the initial CMCH concentration was optimized as 23.8 mg/mL in reaction suspension (i.e. CMCH:Fe_3O_4 = 1:1) to control the thickness of CMCH shell (about 15 nm).

The medium pH is another predominant factor in the course of the binding CMCH, because the pH of the solution can affect the electrical properties of functional groups of Fe_3O_4 particles and CMCH. Typically, The Fe_3O_4 particles could bind with CMCH quite efficiently in the pH range of 6–9 (Fig. 2b). The evident decline of binding capacity at pH > 9.0 is attributed to the deformation of CMCH molecular from sphere shape into chain shape, which leads to a poor solubility. By contrast, and the low uptake at pH < 6.0 may be due to the partial protonation of the active groups and the competition of hydrogen ion with CMCH for binding sites on Fe_3O_4 particles. In this work, we selected the reaction system of pH 7.5 for preparing availably Fe_3O_4@CMCH particles.

It is clear that the reaction time also has a great effect on the coating amount of CMCH on magnetic cores (Fig. 2c). It can be observed that the CMCH uptake approached a maximum at 120 min at the initial CMCH concentration of 23.8 mg/mL (Fe_3O_4: 23.8 mg/mL). However, we discovered that when initial CMCH concentration was increased up to 50 mg/mL, the aggregation distinctly accelerated with the prolonged reaction time under the same experiment conditions. Hence 120 min was considered sufficient to establish equilibrium. Moreover, although the effect of temperature on CMCH coating may exist to some extent, experiments showed that this effect was very little within 293–318 K (Fig. 2d). So Fe_3O_4@CMCH particles were synthesized at 298 K in this work.

Representative TEM images of the as-prepared Fe_3O_4 are shown in Fig. 3a. As is well seen, the average diameter of the magnetic bead is about 150 nm, which is in accordance with the average crystallite size calculated from the XRD pattern (3 1 1) in Fig. 4A(a) based on the Scherrer equation (Wu, Yu, & Fu, 2006). The FTIR spectrum of the as-prepared Fe_3O_4 particles is shown in Fig. 4B(a), which can be observed bands presented at 590 and 3400 cm^{-1} related to the Fe—O vibration and the O—H stretching vibrations, respectively (Xuan, Wang, Yu Jimmy, & Leung Ken, 2009).

The multifunctional modification of core/shell magnetic particle surface with semiconductor material is a fashionable topic due to tailored properties. The effective formation of shell on magnetic cores is a first important step. The shell plays a connective role between magnetic cores and QDs, and protects magnetic cores from corrosion. The hydroxyls on Fe_3O_4 surface provide the favorable condition for CMCH coating. It can be seen clearly in Fig. 3b that the edge of Fe_3O_4@CMCH particles was uneven, and there was a thin layer of fluffy CMCH (about 15 nm) adhered to magnetic bead by a scale of TEM while TEM images were taken, which could provide larger surface area for subsequent CdTe loading. Furthermore, the intensity of Fe_3O_4 diffraction peaks of Fe_3O_4@CMCH composites was weaker than those of pure Fe_3O_4 based on XRD pattern (Fig. 4A(b)), which manifested the presence of amorphous materials (CMCH) on the surface of Fe_3O_4 core. The FT-IR spectrum of Fe_3O_4@CMCH appeared two peaks at 1550 and 1400 cm^{-1} corresponding to the carboxyl antisymmetrical vibration and carboxyl symmetric vibration (Fig. 4B(b)). We also observe a peak at 590 related to the Fe—O vibration which did not exist in pure CMCH (Fig. 4B(f)). These results showed that magnetic particles were coated successfully by CMCH.

3.2. Preparation and characterization of CLMNPs

The positively charged Fe_3O_4@CMCH nanospheres are in favor of binding with negatively charged TGA-capped CdTe nanocrystals by electrostatic attraction. Furthermore, this binding was greatly promoted by complexation between amino groups in CMCH and CdTe. However, the fluorescence intensity of as-prepared LMNPs was strongly affected by pH, temperature, irradiation treatment, and concentration ratio of precursors in the course of synthesis. In our work, the systematic researches about the effect of the four parameters on the PL intensity of LMNPs were carried out.

Effect of pH on the PL intensity of LMNPs was presented in Fig. 5a. It is clear that there were signs of a little fluctuation of the PL intensity of as-prepared LMNPs when pH value of the medium was 7–9,

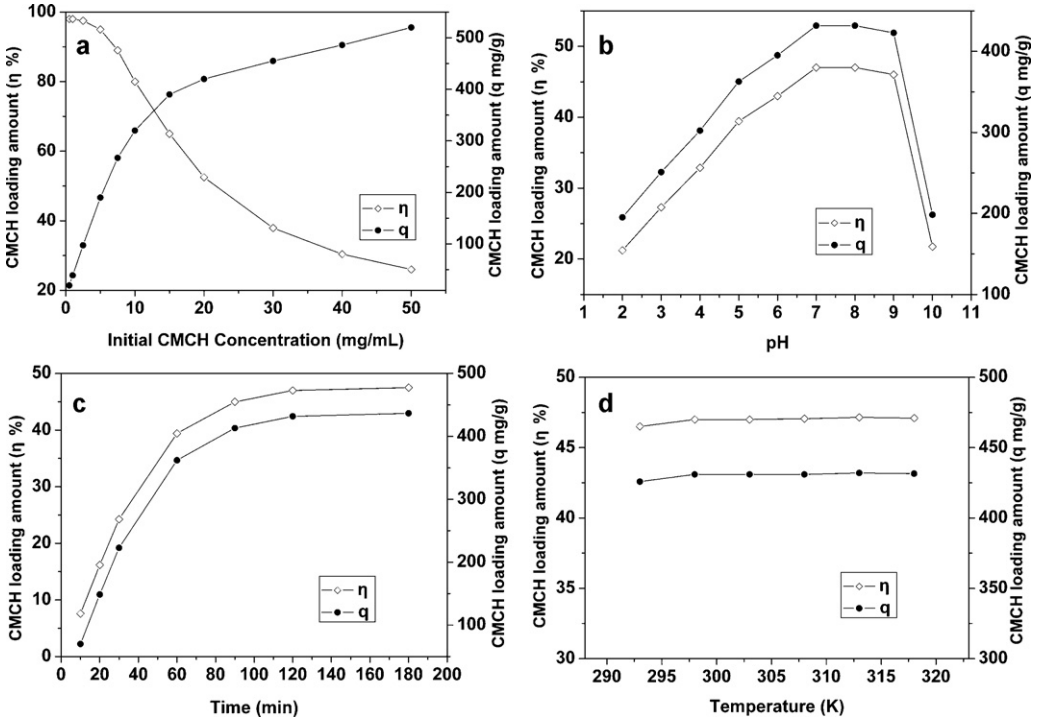

Fig. 2. The loading amount (η% or q mg/g) of CMCH on Fe_3O_4 at different (a) initial CMCH concentration; (b) pH; (c) reaction time; (d) temperature. The other constant conditions except single varied parameter: initial CMCH concentration = 23.8 mg/mL, pH 7.5, reaction time = 120 min, temperature = 298 K, adsorbent = 23.8 mg/mL; vibration speed = 200 rpm.

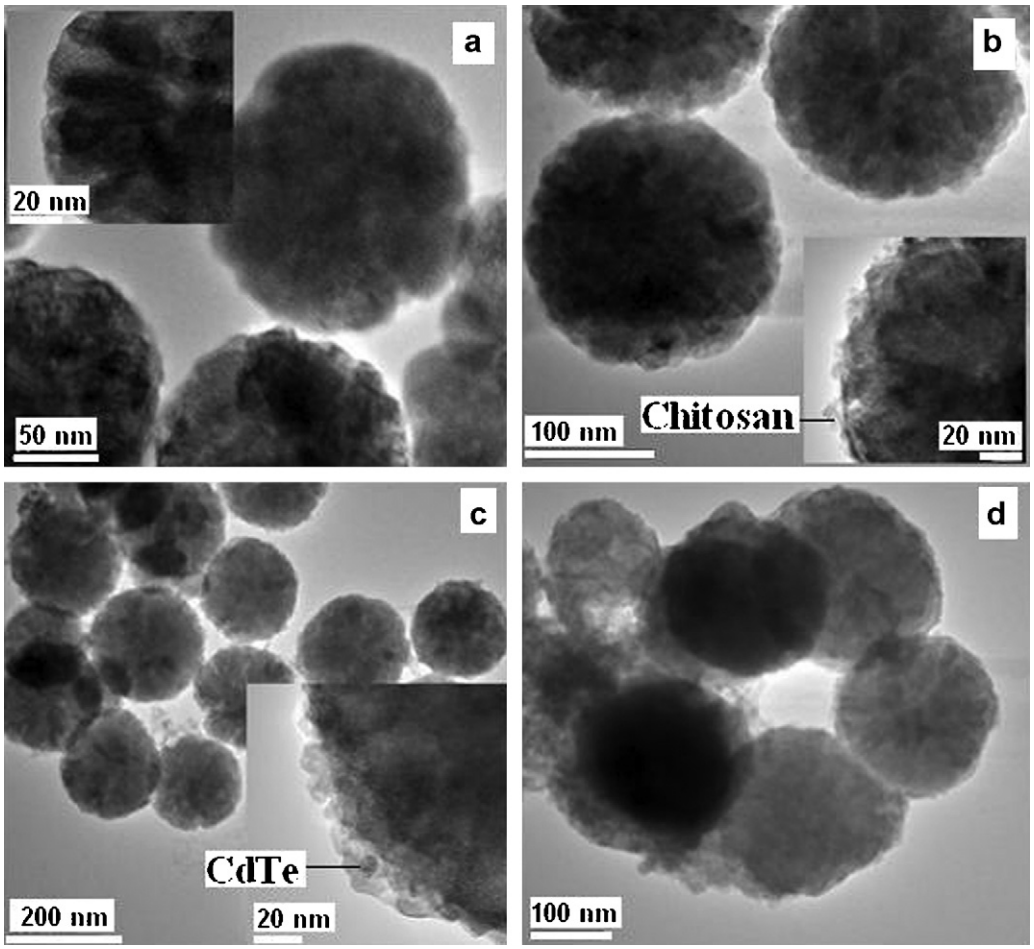

Fig. 3. Transmission electron micrograph (TEM) images of (a) Fe_3O_4 particles, (b) Fe_3O_4@CMCH particles, (c) LMNPs and (d) CFLMNPs.

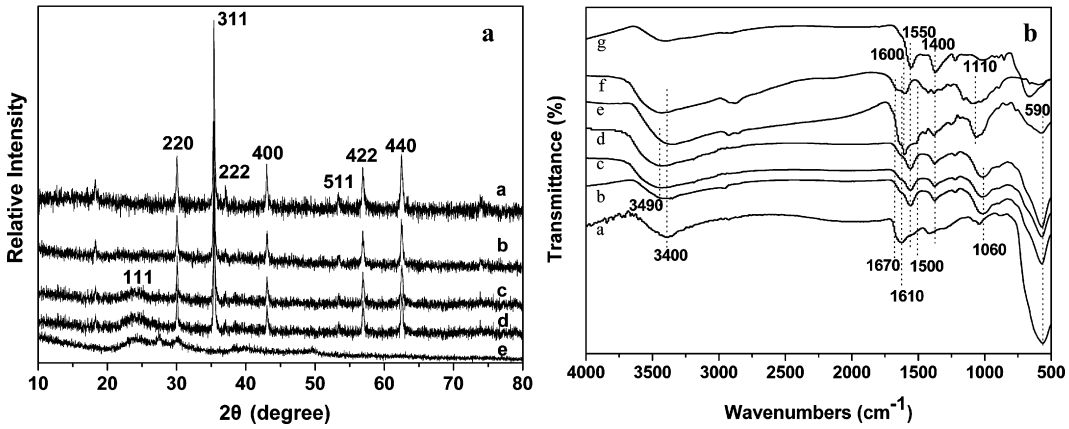

Fig. 4. The characterization of the step-by-step products. (A) XRD patterns of the as-prepared (a) Fe_3O_4, (b) Fe_3O_4@CMCH, (c) LMNPs, (d) CFLMNPs, and (e) CdTe. (B) FT-IR spectra of (a) Fe_3O_4, (b) Fe_3O_4@CMCH, (c) LMNPs, (d) CLMNPs, (e) CFLMNPs, (f) CMCH and (g) CdTe-QDs nanocrystals.

and the intensity reached the highest value in this pH range. Nevertheless, the intensity sharply dropped in the acid range (pH < 7.0), and even nearly quenching below pH 4. This may be because the stability of CdTe QDs was destroyed at low pH, in turn, leaded to difficulty of QDs loading. The decline of PL intensity in alkali solution (pH > 9) may be attributed to formation of cadmium hydroxide (Prelot et al., 2002). Thus, in our preparation system, the binding of CdTe-QDs onto Fe_3O_4@CMCH particles was maintained in the pH 7.5.

Besides, the PL intensity of resulting LMNPs depended on reaction temperature to a great extent. When the temperature gradually rose from 278 K to 328 K in the reaction of uploading CdTe, the PL intensity of products clearly decreased, only accounting for initial 54%, and meanwhile showed the red shift (around 6 nm, Fig. 5b). The possible reason is that trap energy level is malfunction due to change of the surface trap sites of CdTe QDs at high temperature (Biju, Makita, & Sonoda, 2005). The red shift of fluorescence emission peak may be the dipolar-dipolar interaction interior quantum dots (Gardner, Gallardo, & Bertoni, 2006). So it is reasonable to upload CdTe nanocrystal onto Fe_3O_4@CMCH nanospheres at low temperatures.

The light activation of quantum dots before immobilization is another key step to obtain LMNPs with high fluorescence intensity. Fig. 5c indicated the PL intensity of LMNPs prepared using activated CdTe QDs by natural light irradiation treatment in different time periods. Generally speaking, the fluorescence intensity of LMNPs increased with increased irradiation time of the precursor CdTe QDs. Although UV–vis absorbance value of pure QDs solution showed hardly any fluctuations before and after irradiated, the PL intensity of QDs irradiated for 24 h was approximately 3.3 times higher than that of the raw QDs. Accordingly, the PL intensity of the LMNPs prepared using irradiated QDs was 1.2 times

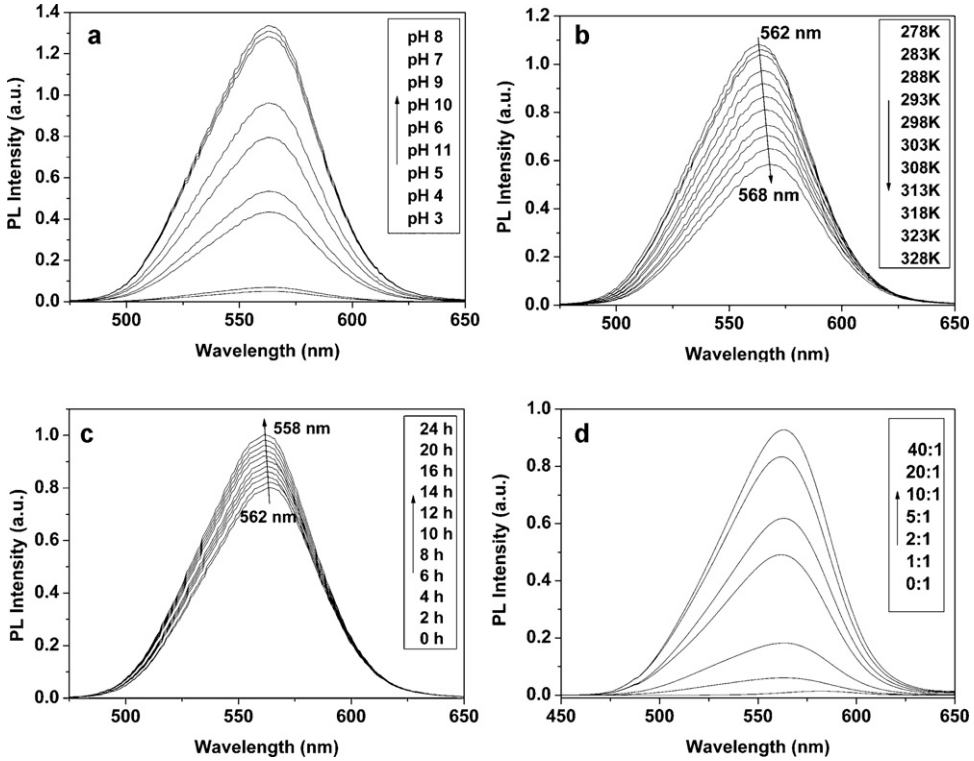

Fig. 5. Fluorescence emission spectra (λ_{ex} = 450 nm) of LMNPs prepared at different (a) medium pH; (b) temperature; (c) light irradiation time of QDs precursor; (d) the QD:Fe_3O_4 ratios. The other constant conditions except single varied parameter: pH 7.5; temperature = 278 K; light irradiation time = 24 h; the QD:Fe_3O_4 ratio = 20:1.

higher than that prepared using unactivated QDs (Fig. 5c), and showed blue shift (about 4 nm). Wang et al. (2004) believed that the light activation could remove the flaws of the surface trap in QDs. We consider that optical irradiation facilitated decomposition of TGA into S^{2-} ions, and then formed CdS shell on CdTe surface. The growing CdS shell greatly improved the surface trap structure of CdTe QDs, consequently, the PL intensity was enhanced obviously.

The PL spectra of the LMNPs prepared under the various QD:Fe_3O_4 ratios were shown in Fig. 5d. Depending on the QD:Fe_3O_4 ratios of preparation, the PL intensity could be significantly varied. Typically, high QD:Fe_3O_4 ratios, i.e., 40:1, corresponding to more amounts of CdTe QDs bound onto the particles, led to a strong PL intensity. On the contrary, in the case of the LMNPs prepared under a low QD:Fe_3O_4 ratio, i.e., 1:1, the PL intensity were markedly weak.

The direct proof of the fabrication of the LMNPs was presented in TEM (Fig. 3c). We can see clearly that the surface of LMNPs was more uneven than that of Fe_3O_4@CMCH particles, and there was CdTe nanocrystal existed in CMCH gauffer. It can be observed that the average diameter of LMNPs was approximately 170 nm. Based on XRD pattern (Fig. 4A(e)), the (1 1 1) peak was the characteristic peak of CdTe nanocrystal which showed preferred orientation in the cubic plane. The peak was also in XRD spectra of LMNPs (Fig. 4A(c)), which directly indicated the success of CdTe immobilization.

The FT-IR spectra of LMNPs and pure CdTe were presented in Fig. 4B(c and g). There were several differences between them. Firstly, The FT-IR spectrum of LMNPs (Fig. 4B(c)) showed that the broad peak at 3400 cm^{-1}, corresponding to the stretching vibration of hydroxyl, amino and amide groups, shifted obviously to higher wave numbers (3490 cm^{-1}) and became wider and stronger, which indicated the strong interaction between these groups and CdTe. Secondly, the FT-IR spectrum of CMCH itself (Fig. 4B(f)) showed two amide bands at 1670 and 1610 cm^{-1}, while amide band at 1670 cm^{-1} has disappeared except amide band at 1610 cm^{-1} became weak in LMNPs (Fig. 4B(c)), which may attribute to complexation and electrostatic attraction between amino groups and thiol-capped CdTe. Thirdly, we also find that the peak situated at 1110 cm^{-1} in pure CMCH (Fig. 3f) related to C—O stretching turned to lower wave number 1060 cm^{-1} in LMNPs (Fig. 4B(c)), while this peak became stronger than pure CdTe (Fig. 4B(g)). These results confirmed that CdTe quantum dots were well immobilized onto the Fe_3O_4@CMCH particles to form the LMNPs.

It is inevitable to expose resulting LMNPs to aqueous solution in the subsequent course of loading and release of drug. In order to protect CdTe on LMNPs from decomposition in water soluble, in this work, CMCH was selected to prepare CMCH-coated LMNPs (CLMNPs). The outer CMCH shell had other advantages. The capsulation of QDs within the CMCH shell could prolong fluorescence lifetime of the QDs, alleviate the toxicity of the QDs in biological environments, and at the same time the CMCH molecules could provide ideal functional groups for folate binding and drug adsorption. As already noted, the thickness of the CMCH shell can be adjusted to about ten nanometers by optimizing the initial CMCH concentration, pH, reaction time and temperature.

3.3. Preparation and characterization of CFLMNPs

To obtain folate-conjugated CLMNPs, the amino groups of the CMCH outer shell on the surface of CLMNPs were coupled with γ-carboxyl group of folate by the amide linkage. The coupling reaction was performed in PBS at room temperature in the presence of EDAC and NHS as the activating agent for the carboxylic group.

The morphology of the resulting CFLMNPs was showed in TEM image (Fig. 3d) and SEM image (SD 1a). The average diameter of the CFLMNPs was determined to be about 170–190 nm by TEM (SD 1b). Compared with the average diameters of LMNPs, those of CFLMNPs increased by about 10 nm. This result was compatible with data calculated from the XRD pattern (3 1 1) in Fig. 4A(d) according to the Scherrer equation. Furthermore, the intensity of Fe_3O_4 diffraction peaks of the CFLMNPs was weaker than those of the previous products based on XRD pattern (Fig. 4A(b, c and d)), which reflected the presence of more amorphous materials (CMCH and FA) on the surface of the CFLMNPs. Based on FTIR spectrum of the CFLMNPs (Fig. 4B(e)), two absorption peaks at 1600 cm^{-1} and 1500 cm^{-1} were the characteristic absorption peaks of the benzene ring on the folate, confirming successful synthesis of the CMCH-based folate/luminescent/magnetic nanoparticles. The X-ray energy dispersive (EDX) analysis indicated that the elemental compositions of the CFLMNPs were primarily Fe, O, Cd, Te, C, N and S, which further confirmed the structure ingredients of the CFLMNPs. According to the photographs before and after CdTe QDs binding onto MNPs (inset in Fig. 6A), the color conversion at 365 nm from bright yellow into orange red showed the realization of effective reaction, at the same time, the achievement of magnetic nanocomposites with fluorescence of orange red color also verified success of immobilization. All the above results suggest that CFLMNPs have been successfully prepared.

The magnetic properties of the CFLMNPs synthesized through layer-by-layer assembly were also measured using a vibrating sample magnetometer (VSM). As shown in the VSM magnetization curves (Fig. 6A), with step-by-step fabrication, the saturation magnetization declined accordingly due to the thickening of the shells. The saturation magnetization of CFLMNPs (45.6 emu/g) accounted for about 54.8% of that of the Fe_3O_4 core (83.2 emu/g). The as-prepared CFLMNPs showed a superparamagnetic property at room temperature and possessed adequate magnetic responsiveness in the applications for magnetic separation and biomedicine.

Fig. 6B evaluated the effect of NaCl concentration on the size and stability of CFLMNPs. As presented in DLS data (Fig. 6B), firstly, the mean diameters of CFLMNPs showed relatively small fluctuation and was about 170–190 nm in PBS containing 100–200 mM NaCl (pH = 5.3 and pH 7.4), which was consistent with the results detected from TEM and indicated monodisperse particles. This was mainly because CMCH shell would bring more ions in a dilute salt solution, which led to electrostatic repulsion and low viscosity, in turn, aggregation of particles was restrained. Secondly, particles showed much bigger average diameter from DLS data (200–300 nm) than from TEM images in store medium containing NaCl concentrations of 200–500 mM, indicating possible aggregation. This could come down to competition of excess salt with CMCH for water molecules in solution, even in CMCH shell, which resulted in relatively high viscosity, in turn, particles aggregated. Thirdly, under the same salt concentration, the particle sizes in medium at pH 5.3 were less than at pH 7.4. This could be attributed to electrostatic shielding of CMCH shell because of introduction of excessive like charges in a relatively acid environment. The electrostatic shielding led to shrink of individual polymer and decline of intermolecular entangled degree, accordingly, the CFLMNPs were more stable at pH 5.3 than at pH 7.4. In terms of the biokinetics, the desired sizes distribution of particles as a drug carrier should range from 10 nm to 200 nm (Win & Feng, 2005). The ultrafine particles (typically, less than 10 nm) casually slip away from nephridium tissue, whereas the micrometer-sized particles tend to reduce cell permeability. So the size distribution of CFLMNPs were within the allowable range for cell permeability under simulate cancer or normal physiological environment and are desirable for drug carriers to extend their blood circulation time. The sizes of CFLMNPs were more desirable in the acidic solution containing low salt. Similarly, the stability of intermediate products was also affected by NaCl content in growth medium. In this work, we synthesized and stored CFLMNPs in PBS containing 100 mM NaCl all along to obtain stable nanoparticle (150–190 nm).

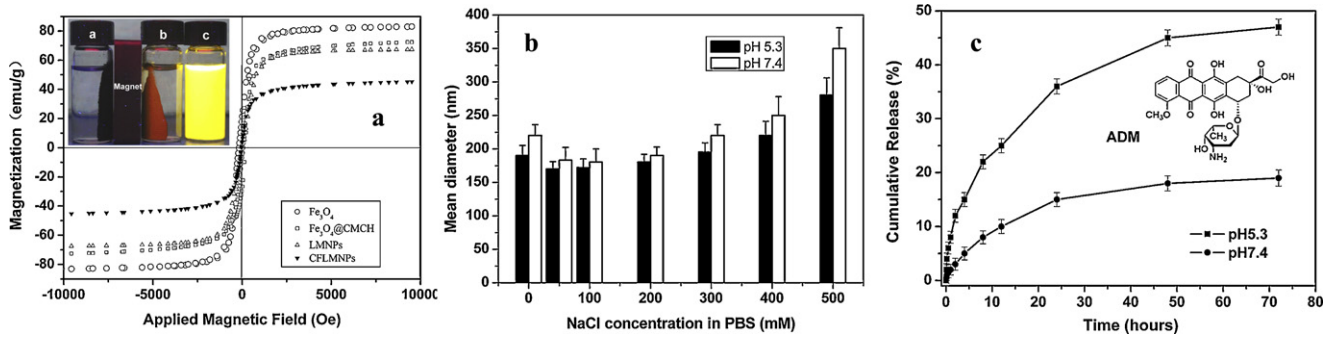

Fig. 6. Characterization and evaluation of CFLMNPs. (A) VSM magnetization curves of the step-by-step products in applied magnetic field at 305 K. The inset in left top show photographs taken under a 365 nm UV lamp: (a) Fe_3O_4 particles, (b) CFLMNPs, (c) CdTe QDs. (a) and (b) are attracted by a permanent magnet. (B) The DLS data of CFLMNPs stored in PBS containing different NaCl content. (C) Release profiles of ADM from ADM-loaded CFLMNPs in PBS solutions of pH 5.3 and pH 7.4 at 37 °C.

3.4. Drug loading and pH-regulated release properties in vitro

Under present experiment condition, the loading efficiency of ADM was 36.6 wt% for CFLMNPs, namely the actual loading amount of ADM on the CFLMNPs was approximately 439.2 mg/g. ADM molecule contains both acidic phenolichydroxyl groups and alkaline amino groups (Fig. 6c inset) that are capable to interact with the amino groups and hydroxy on chitosan shell of as-synthesized CFLMNPs to form intermolecular complexes by hydrogen bonding, additionally, there was physical adsorption due to the mucosity of the chitosan shell, resulting in a high drug loading efficiency.

The release process under sink condition was examined in a simulated normal body fluid (PBS, pH 7.4) and an acidic environment (PBS, pH 5.3) at 37 °C. Fig. 6C showed the release profiles of ADM from the ADM-loaded CFLMNPs into outer aqueous phase. As shown in Fig. 6C, the cumulative release mainly occurred for the first 24 h under two pH systems, and could reach 36% at pH 5.3 and 15% at pH 7.4 within 24 h, respectively. However, the cumulative release only reached 47% at pH 5.3 and 19% at pH 7.4, respectively, even though the release continued for 72 h. We partly attributed this incomplete ADM release to the moderate hydrophobicity of ADM with water solubility of ~1 mg/mL. In addition, the outer irregular CMCH shell might be one of reasons why ADM molecules could insert into shell gauffer, and some ADM molecules might even be deposited deeply on the surface of Fe_3O_4 core. This displayed relatively slow release kinetics. The research also showed that the continued release process at pH 7.4 was much slower than that at pH 5.3. One of possible reasons was the low solubility of ADM at pH 7.4 where it was unfavorable to dissociate ADM from the ADM-loaded CFLMNPs. By contrast, the release at pH 5.3 was more favorable than that at pH 7.4 because the solubility of ADM at pH 4–5.5 is optimum. Another possible reason would be the water content of the CMCH shell. When at pH 5.3, CMCH polymer is easily soluble to water, so the water content of the shell would be high, and accordingly the permeability of ADM would be higher. On the other hand, when at pH 7.4, the solubility of CMCH polymer is relatively low, so the water content of the shell would be low, and accordingly the permeability of ADM would be lower. This is exactly what we expect, i.e., ADM could principally be distributed around tumor tissues (acidic microenvironment) rather than located in normal section. Thus, the multifunctional CFLMNPs hold a promise as a pH-regulated release delivery vehicle for potential cancer therapy.

3.5. Cytotoxicity studies in vitro

To examine cytotoxicity and tumor targeting of CFLMNPs, human hepatocytes L02 (normal) and HepG2 (cancer) cell lines were chosen to incubate with blank and ADM-loaded CFLMNPs in vitro. The results showed relatively high cell viability in two cell lines at different blank CFLMNPs concentration (Fig. 7 unfilled bar). 85% and 70% of viability of L02 and HepG2 cells were watched even at a blank CFLMNPs concentration of 1 mg/mL, respectively, which reveals a low cytotoxicity and favorable cell compatibility for CFLMNPs. However, a drastic decrease (Fig. 7 filled bar) in cell viability can be observed when the cells were incubated with ADM-loaded CFLMNPs for 12 h even at a concentration as low as 200 μg/mL (ADM-loaded CFLMNPs), which may be attributed to damage of ADM on nanocarriers to cells rather than harm of nanocarriers to those. These results show

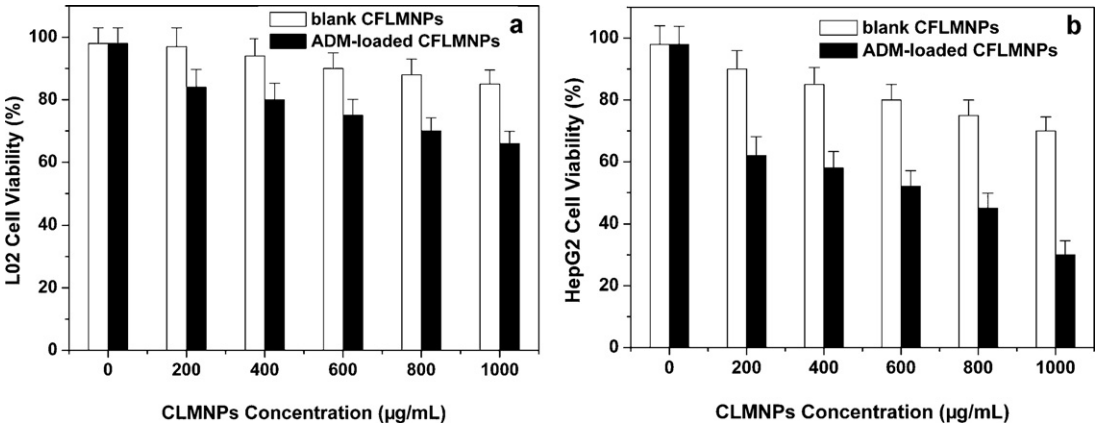

Fig. 7. In vitro cytotoxicity of blank CFLMNPs (unfilled bar) and ADM-loaded CFLMNPs (filled bar) at different concentrations against L02 cells (a) and HepG2 cells (b) after 12 h incubation. The control experiment was performed in the absence of nanocarriers.

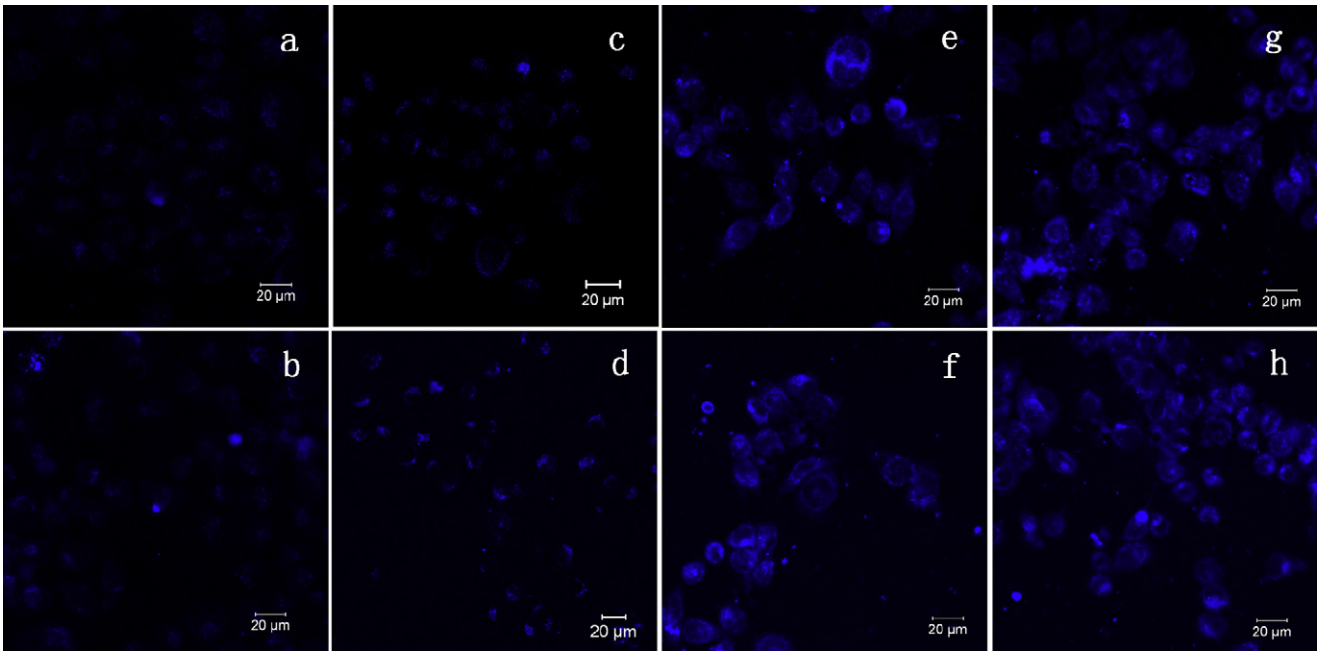

Fig. 8. Laser scanning confocal images of representative L02 cells and HepG2 cells incubated with blank and ADM-loaded CFLMNPs with a concentration of 200 μg/mL for 30 min (top) and 60 min (bottom), respectively. (a, b) L02 cells incubated with blank CFLMNPs; (c, d) L02 cells incubated with ADM-loaded CFLMNPs; (e, f) HepG2 cells incubated with blank CFLMNPs; (g, h) HepG2 cells incubated with ADM-loaded CFLMNPs. Excitation laser wavelength = 405 nm.

that the released ADM from the ADM-loaded CFLMNPs still hold high anticancer activity. In addition, the viability of the HepG2 cells was much lower than that of the L02 cells after incubated with corresponding carriers, which demonstrates that CFLMNPs possess higher growth inhibition property for cancer cell than for normal cell due to folate receptor-mediated specific endocytosis.

3.6. Cellular imaging

After confirmed the powerful fluorescence using a fluorescence microscopy upon excitation with a wavelength of 488 nm, the blank and ADM-loaded CFLMNPs were added to L02 cells and HepG2 cells to incubate for observations of binding and morphological changes of the cells. In order to avoid the fluorescent interference inducted by ADM as well as possible, we observed cell imaging at an excitation laser wavelength of 405 nm. The first control experiment was performed to ensure there was no distinct autofluorescence from the cell itself under similar condition. The second control experiment has been also carried out to make clear differences in transportation mechanism for free ADM and drug carrier. It is found that the cellular uptake of free ADM was faster than that of blank CFLMNPs (SD 2a and b) through comparing fluorescence within the cells, indicating that the transportation of the free ADM was a passive diffusion mechanism (Yoo & Park, 2004). Furthermore, The free ADM was dramatically accumulated in the nucleus due to rapid binding of the free ADM to the chromosomal DNA (Gabbay et al., 1976; Prabaharan, Grailer, Pilla, Steeber, & Gong, 2009), while after endocytosed by the cells, the CFLMNPs were mainly located in cytoplasm due to the big sizes of the CFLMNPs. In the case of the ADM-loaded CFLMNPs (SD 2c), the fluorescence within the cells is more intense comparing with free ADM or CFLMNPs alone due to the integration effects of ADM and CFLMNPs in ADM-loaded CFLMNPs. However, the particles were still mainly located in cytoplasm. Thus, the fluorescence crosstalk from the free ADM can be eliminated by comparing the distribution of intracellular fluorescence.

Fig. 8 presented the typical scanning confocal microscopy images of the L02 cells and the HepG2 cells after stained with the nanocarriers for 30 and 60 min at a concentration of 200 μg/mL (blank or ADM-loaded CFLMNPs), respectively. Firstly, it is clear that the amount of distributing nanocarriers (blank and ADM-loaded CFLMNPs) within the HepG2 cells was much higher than within the L02 cells under corresponding condition. In order to make certain this mechanism, the third control experiment has been performed with non-folate-conjugated CLMNPs. In the case of non-folate-conjugated particles, it is found that the nanoparticles could also enter the cells, and that the cellular uptake of the particles were consistent within two kinds of the cells (SD 3). This may be because the non-folate-conjugated particles were transported into cells through a non-specific endocytosis process. In this case, the smart nanoparticles should play a critical role in the course of their overcoming cell membrane obstacles to enter the intracellular region. By contrast, the uptake of folate-conjugated particles (blank CFLMNPs) into HepG2 cells (Fig. 8e and f) was more significant than into L02 cells (Fig. 8a and b), indicating that the cellular uptake of the particles into HepG2 cells can be facilitated by conjugating folate on their surface. In fact, the folate-conjugated particles were transported into the HepG2 cells by an folate-receptor-mediated endocytosis mechanism due to high expression of folate receptor on the surface of tumor cell membrane. Additionally, the sizes of CFLMNPs were slightly smaller at pH 5.3 than at pH 7.4 (Fig. 6B), the CFLMNPs were easier to access to the cancers cell. Secondly, the smart CFLMNPs can been transported into the intracellular section and illumined the cells. The cellular images showed that no signs of morphological destruction could be found after treatment with the blank CFLMNPs for 60 min (Fig. 8f), which suggests that there was a membrane endocytosis mechanism with no apparent bilayer damage. Thirdly, after endocytosed by the cells, the CFLMNPs were mainly located in cytoplasm, reflecting the big sizes of the CFLMNPs so that the particles could not readily enter into organelles. In addition, there were agglomerate light clusters inside the cell, and the bright spots amplified with increased incubation time. We speculate that significant aggregation of particles in

the cytosol can be attributed to protein adsorption by big-sized CFLMNPs. It is also possible to expose CdTe QDs in chitosan gauffer to cytoplasm, which provided the occasion of reacting with certain specific proteins or enzyme in cells (Weng et al., 2006). Whether it was protein adsorption or specific reaction, the results leaded to a nonuniform distribution of fluorescence in cells. Finally, the signs of cell deformation were observed when the HepG2 cells were exposed to ADM-loaded CFLMNPs, especially after long time incubation (Fig. 8h). This indicates that ADM may have worked in this case, which was in consistent with assay of cell viability.

4. Conclusions

In this study, we presented a rational method of preparing folate conjugated carboxymethyl chitosan@luminescent@magnetic nanoparticles by layer-by-layer assembly technique. It was found that the coating amount and binding mode of CMCH were strongly influenced by initial CMCH concentration, medium pH, and reaction time. The PL intensity of the resulting CFLMNPs increased obviously when the reaction system was maintained in a slightly alkalescent, relatively low temperature, a proper QD:Fe_3O_4 ratio, and moderate light activation to precursor CdTe QDs. The outer CMCH shell with good functionality provided not only protection from CdTe QDs' escape and fluorescent quenching but also a potent platform for folate modifying and drug binding. The results showed that as-synthesized CFLMNPs possess superparamagnetic ability and intense PL property, and are stable under simulate physiological environment. Furthermore, the folate receptor-mediated specific targeting and pH-regulated release profile of ADM from ADM-loaded CFLMNPs have been found in vitro, which could presage to allow drug for the preferential distribution around tumor. It can draw a conclusion that multifunctional quaternary nanoparticles designed as a targeting probe for cancer cells could potentially provide an approach for diagnosis, drug delivery, and real-time detection on drug treatments of the intracellular processes.

Acknowledgments

This study was supported by the National Natural Science Foundation of China Fund (No. 21105039), and the Fundamental Research Funds for the Central University (No. lzujbky-2012-k09).

Appendix A. Supplementary data

Supplementary data associated with this article can be found, in the online version, at doi:10.1016/j.carbpol.2011.11.087.

References

Biju, V., Makita, Y., & Sonoda, A. (2005). Temperature-sensitive photoluminescence of CdSe quantum dot clusters. *Journal of Physical Chemistry B*, *109*, 13899–13905.
Blum, R. H., & Carter, K. S. (1974). New antitumor drug with significant clinical activity. *Annals of Internal Medicine*, *80*, 249–259.
Calero, N., Munoz, J., Ramírez, P., & Guerrero, A. (2010). Flow behaviour, linear viscoelasticity and surface properties of chitosan aqueous solutions. *Food Hydrocolloids*, *24*, 659–666.
Chang, Y. C., & Chen, D. H. (2005). Preparation and characterization of chitosan poly (acrylic acid) magnetic microspheres. *Journal of Colloid and Interface Science*, *283*, 446–451.
Chen, J. P., Yang, P. C., Ma, Y. H., & Wu, T. (2011). Characterization of chitosan magnetic nanoparticles for in situ delivery of tissue plasminogen activator. *Carbohydrate Polymers*, *84*, 364–372.
Chen, X. G., & Park, H. J. (2003). Preparation and rheological properties of deoxycholate-chitosan and carboxymethyl-chitosan in aqueous systems. *Carbohydrate Polymers*, *53*, 355–359.
Cho, H. S., Dong, Z. Y., Pauletti, G. M., Zhang, J. M., Xu, H., Gu, H. C., et al. (2010). Fluorescent, superparamagnetic nanospheres for drug storage, targeting, and imaging: A multifunctional nanocarrier system for cancer diagnosis and treatment. *Nano*, *4*, 5398–5404.
Corato, R. D., Bigall, N. C., Ragusa, A., Dorfs, D., Genovese, A., Marotta, R., et al. (2011). Multifunctional nanobeads based on quantum dots and magnetic nanoparticles: Synthesis and cancer cell targeting and sorting. *Nano*, *5*, 1109–1121.
Deng, H., Li, X. L., Peng, Q., Wang, X., Chen, J. P., & Li, Y. D. (2005). Monodisperse magnetic single-crystal ferrite microspheres. *Angewandte Chemie International Edition*, *44*, 2782–2785.
Fisher, Huddersman, K. A., Taylor, K. D., & Joan, M. (2003). Comparison of micro- and mesoporous inorganic materials in the uptake and release of the drug model fluorescein and its analogues. *Chemistry-A European Journal*, *9*, 5873–5878.
Gabbay, E. J., Grier, D., Fingerie, R. E., Reimer, R., Levy, R., & Pearce, S. W. (1976). Interaction specificity of the anthracyclines with DNA. *Biochemistry*, *15*, 2062–2070.
Gardner, H. C., Gallardo, D. E., & Bertoni, C. (2006). Temperature shifted photoluminescence in CdTe nanocrystals. *Proceedings of SPIE*, *6195*, 61950N1-8
Gil, P. R., & Parak, W. J. (2008). Composite nanoparticles take aim at cancer. *Nano*, *2*, 2200–2205.
Guo, J., Yang, W. L., & Wang, C. C. (2005). Systematic study of the photoluminescence dependence of thiol-capped CdTe nanocrystals on the reaction conditions. *Journal of Physical Chemistry B*, *109*, 17467–17473.
Guo, J., Yang, W. L., Wang, C. C., He, J., & Chen, J. Y. (2006). Poly(N-isopropylacrylamide)-coated luminescent/magnetic silica microspheres: Preparation, characterization, and biomedical applications. *Chemistry of Materials*, *18*, 5554–5562.
Jayakumar, R., Menon, D., Manzoor, K., Nair, S. V., & Tamura, H. (2010 a). Biomedical applications of chitin and chitosan based nanomaterials—A short review. *Carbohydrate Polymers*, *82*, 227–232.
Jayakumar, R., Prabaharan, M., Nair, S. V., Tokura, S., Tamura, H., & Selvamurugan, N. (2010). Novel carboxymethyl derivatives of chitin and chitosan materials and their biomedical applications. *Progress in Materials Science*, *55*, 675–709.
Jeong, Y. I., Na, H. S., Cho, K. O., Lee, H. C., Nah, J. W., & Cho, C. S. (2009). Antitumor activity of adriamycin-incorporated polymeric micelles of poly(γ-benzyl L-glutamate)/poly(ethylene oxide). *International Journal of Pharmaceutics*, *365*, 150–156.
Mangeney, C., Bousalem, S., Connan, C., Vaulay, M., Bernard, S., & Chehimi, M. M. (2006). Latex and hollow particles of reactive polypyrrole: Preparation, properties, and decoration by gold nanospheres. *Langmuir*, *22*, 10163–10169.
Manzoor, K., Johny, S., Menon, D., & Nair, S. V. (2009). Bioconjugated luminescent quantum dots of doped ZnS:Mn a cytofriendly system for targeted cancer imaging. *Nanotechnology*, *20*, 065102.
Mathew, M. E., Mohan, J. C., Manzoor, K., Nair, S. V., Tamura, H., & Jayakumar, R. (2010). Folate conjugated carboxymethyl chitosan-manganese doped zinc sulphide nanoparticles for targeted drug delivery and imaging of cancer cells. *Carbohydrate Polymers*, *80*, 442–448.
Miller, G. L. (1959). Use of dinitrosalicylic acid reagent for determination of reducing sugar. *Analytical Chemistry*, *31*, 426–431.
Muzzarelli, R. A. A., Boudrant, J., Meyer, D., Manno, N., DeMarchis, M., & Paoletti, M. G. (2012). Current views on fungal chitin/chitosan, human chitinases, food preservation, glucans, pectins and inulin: A tribute to Henri Braconnot, precursor of the carbohydrate polymers science, on the chitin bicentennial. *Carbohydrate Polymers*, *87*, 995–1012.
Myers, R. R., Campana, W. M., & Shubayev, V. I. (2006). The role of neuroinflammation in neuropathic pain: Mechanisms and therapeutic targets. *Drug Discovery Today*, *11*, 8–20.
Pan, J., & Feng, S. S. (2009). Targeting and imaging cancer cells by folate decorated quantum dots loaded nanoparticle of biodegradable polymers. *Biomaterials*, *30*, 1176–1183.
Prabaharan, M., Grailer, J. J., Pilla, S., Steeber, D. A., & Gong, S. Q. (2009). Gold nanoparticles with a monolayer of doxorubicin-conjugated amphiphilic block copolymer for tumor-targeted drug delivery. *Biomaterials*, *30*, 6065–6075.
Prelot, B., Janusz, W., Thomas, F., Villieras, F., Charmas, R., Piasecki, W., et al. (2002). Adsorption of cadmium ions at the electrolyte/silica interface: Experimental study of surface properties. *Applied Surface Science*, *196*, 322–330.
Rejinold, N. S., Chennazhi, K. P., Tamura, H., Nair, S. V., & Jayakumar, R. (2011). Multifunctional chitin nanogels for simultaneous drug delivery, bioimaging and biosensing. *ACS Applied Materials & Interfaces*, *3*, 3654–3665.
Saleh, N., Phenrat, T., Sirk, K., Dufour, B., Ok, J., Sarbu, T., et al. (2005). Adsorbed triblock copolymers deliver reactive iron nanoparticles to the oil/water interface. *Nano Letters*, *5*, 2489–2494.
Turek, J. J., Leamon, C. P., & Low, P. S. (1993). Endocytosis of folate–protein conjugates – ultrastructural-localization in Kb cells. *Journal of Cell Science*, *106*, 423–430.
Wang, C., Ma, Q., Dou, W., Kanwal, S., Wang, G. N., Fan, P., et al. (2009). Synthesis of aqueous CdTe quantum dots embedded silica nanoparticles and their applications as fluorescence probes. *Talanta*, *77*, 1358–1364.
Wang, J. S., Peng, R. T., Yang, J. H., Liu, Y. C., & Hu, X. J. (2011). Preparation of ethylenediamine-modified magnetic chitosan complex for adsorption of uranyl ions. *Carbohydrate Polymers*, *84*, 1169–1175.
Wang, Y., Tang, Z., Correa, D. M. A., Pastoriza-Santos, I., Giersig, M., Kotov, N. A., et al. (2004). Polymers as multidentate ligands for surface modification and hierarchical. *Journal of Physical Chemistry B*, *108*, 15461–15469.
Weng, J. F., Song, X. T., Li, L., Qian, H. F., Chen, K. Y., Xu, X. M., et al. (2006). Highly luminescent CdTe quantum dots prepared in aqueous phase as an alternative fluorescent probe for cell imaging. *Talanta*, *70*, 397–402.
Win, K. Y., & Feng, S. S. (2005). Effects of particle size and surface coating on cellular uptake of polymeric nanoparticles for oral delivery of anticancer drugs. *Biomaterials*, *26*, 2713–2722.

Wu, L., Yu, J. C., & Fu, X. (2006). Characterization and photocatalytic mechanism of nanosized CdS coupled TiO_2 nanocrystals under visible light irradiation. *Journal of Molecular Catalysis A: Chemical*, *244*, 25–32.

Xu, X. Q., Deng, C. H., Gao, M. X., Yu, W. J., Yang, P. Y., & Zhang, X. G. (2006). Synthesis of magnetic microspheres with immobilized metal ions for enrichment and direct determination of phosphopeptides by matrix-assisted laser desorption ionization mass spectrometry. *Advanced Materials*, *18*, 3289–3293.

Xuan, S. H., Wang, Y. X. J., Yu Jimmy, C., & Leung Ken, C. F. (2009). Preparation, characterization, and catalytic activity of core/shell Fe_3O_4@polyaniline@Au nanocomposites. *Langmuir*, *25*, 11835–11843.

Yoo, H. S., & Park, T. G. (2004). Folate-receptor-targeted delivery of doxorubicin nano-aggregates stabilized by doxorubicin–PEG–folate conjugate. *Journal of Controlled Release*, *100*, 247–256.